p-p Interactions at 2 Bev. I. Single-Pion Production*

W. J. FICKINGER†
Yale University, New Haven, Connecticut; and Brookhaven National Laboratory, Upton, New York

AND

E. PICKUP,‡ D. K. ROBINSON, AND E. O. SALANT
Brookhaven National Laboratory, Upton, New York

(Received October 13, 1961)

3600 two-pronged events, obtained in p-p interactions at 2 Bev in the BNL 20-in. hydrogen bubble chamber, have been analyzed. Cross sections have been measured for elastic scattering, for the two modes of single-pion production, $p+p\rightarrow p+n+\pi^+$, $p+p\rightarrow p+p+\pi^0$, and for strange-particle production. The branching ratio for the two one-pion production reactions is $\sigma(pn\pi^+)/\sigma(pp\pi^0)=4.17\pm0.25$. Momentum distributions and Q values indicate that single-pion production proceeds almost entirely through the $(\frac{3}{2},\frac{3}{2})$ resonant state. The data have been considered in terms of the extended isobar model and also a one-pion exchange model for production. The branching ratio and momentum distributions can be explained by including a small effect from the $I=\frac{1}{2}$ resonant state in addition to the dominant $I=\frac{3}{2}$ resonance. The c.m. angular distribution of the nucleons in single-pion production shows very marked backward-forward peaking indicating a one-pion exchange mechanism. Absolute differential cross sections as a function of laboratory kinetic energy have been calculated from Selleri's equation for the $pn\pi^+$ reaction. There is good agreement with the data for low four-momentum transfers $[q^2<0.15(\text{Bev}/c)^2]$, but for higher momentum transfers the theoretical cross sections are larger than the experimental cross sections.

I. INTRODUCTION

DURING the past decade, with the advent of high-energy accelerators, several groups have investigated the nature of energetic proton-proton interactions. Measurements of total and elastic p-p cross sections have been made in counter experiments.[1] More specific information on the nature of inelastic processes has been obtained from cloud-chamber experiments.[2] The introduction of the hydrogen bubble chamber technique has advanced this work by providing higher interaction probability, target simplicity, and greater measuring precision. The BNL 20-in. hydrogen bubble chamber was exposed to beams of 2.85- and 2.02-Bev protons at the Cosmotron. Results from the analysis of the 2.85-Bev exposure have been reported by the BNL Bubble Chamber group[3] and by the Yale High Energy group.[4] This paper gives results from the analysis of two-pronged events in the 2.02-Bev exposure.

The two-pronged events comprise elastic scattering events, single- and multiple-pion production, and strange-particle production. Results from multiple pion-production are reported in paper II.[5] Of particular interest in this experiment is single-pion production, which has been compared in detail with the predictions

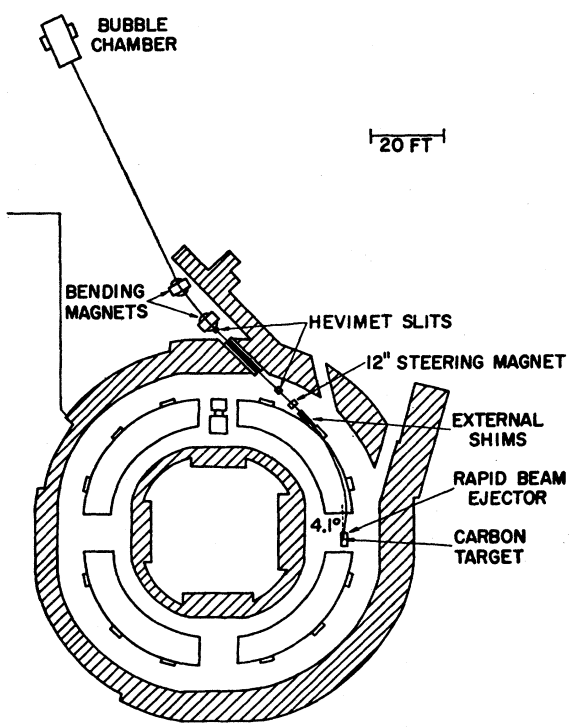

FIG. 1. Plan view of scattered-out 2-Bev proton beam.

* Work performed under the auspices of the U. S. Atomic Energy Commission.

† Now at University of Kentucky, Lexington, Kentucky.

‡ On leave of absence from National Research Council, Ottawa, Ontario, Canada.

[1] L. W. Smith, W. McReynolds, and G. Snow, Phys. Rev. **97**, 1186 (1955); R. W. Wright, G. Saphir, W. M. Powell, G. Maenchen, and W. B. Fowler, *ibid.* **100**, 1802 (1955); F. F. Chen, C. P. Leavitt, and A. M. Shapiro, *ibid.* **103**, 211 (1956); B. Cork, W. A. Wenzel, and C. W. Causey, Jr., *ibid.* **107**, 859 (1957); and M. J. Longo, J. A. Helland, W. N. Hess, B. J. Moyer, and V. Perez-Mendez, Phys. Rev. Letters **3**, 568 (1959).

[2] W. B. Fowler, R. P. Shutt, A. M. Thorndike, W. L. Whittemore, W. T. Cocconi, E. Hart, M. M. Block, and E. M. Harth, Phys. Rev. **103**, 1484 (1956); A. P. Batson, B. B. Culwick, J. G. Hill, and L. Riddiford, Proc. Roy. Soc. (London) **A251**, 218 (1959).

[3] R. I. Louttit, T. W. Morris, D. C. Rahm, R. R. Rau, A. M. Thorndike, W. J. Willis, and R. M. Lea, Phys. Rev. **123**, 1465 (1961).

[4] G. A. Smith, H. Courant, E. C. Fowler, H. Kraybill, J. Sandweiss, and H. Taft, Phys. Rev. **123**, 2160 (1961).

[5] E. Pickup, D. K. Robinson, and E. O. Salant, following paper [Phys. Rev. **125**, 2091 (1962)].

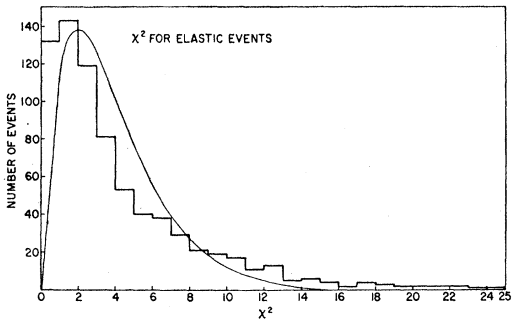

FIG. 2. χ^2 distribution for elastic events. The curve shows the theoretical distribution for four constraints.

of the isobar model of Lindenbaum and Sternheimer[6] and the one-pion exchange model of Selleri.[7]

II. EXPERIMENTAL ARRANGEMENT

Figure 1 shows the layout of the beam at the Cosmotron; this was essentially the same as that used in the 2.85-Bev experiment. The circulating proton beam was deflected on to a carbon target by the rapid beam ejector. Protons scattered at 4° were collimated and momentum-analyzed to give a well-defined beam of 2-Bev protons at the bubble chamber.

The BNL hydrogen bubble chamber is 20 in. long, 10 in. deep, and 9 in. high. The magnetic field was 17 kgauss, and was monitored throughout the run. The use of the rapid beam ejector gave a very short (5 μsec) pulse of protons, and this, together with the excellent working characteristics of the chamber, produced pictures of uniformly high quality, so that precision ionization measurements were possible.

III. ANALYSIS

About 45 000 pictures were taken, giving a total of 57 300 interactions. Of these a sample of 3600 events, found within a well-defined fiducial volume in the chamber, were measured. Half of the events were measured and analyzed at Yale and half at BNL.

The pictures from which this sample was taken were scanned twice and, except for a small-angle elastic scattering correction, the scanning efficiency was estimated to be almost 100%.

The events were measured with digitized equipment, and were analyzed using the YAP and TRED spatial reconstruction programs, and the GUTS kinematic analysis program[8] for the IBM-704 computer. The measuring error was about 35 μ in the bubble chamber which, for a 1-Bev/c proton with 20-cm track length, corresponds to a 20-Mev/c uncertainty in the momentum determination.

[6] R. M. Sternheimer and S. J. Lindenbaum, Phys. Rev. **123**, 333 (1961).

[7] F. Selleri, Phys. Rev. Letters **6**, 64 (1960).

[8] J. P. Berge, F. T. Solmitz, and H. D. Taft, University of California Radiation Laboratory Report UCRL-9097, 1960 (unpublished).

The mean beam momentum was determined from the measurement of long beam tracks in the bubble chamber, giving $P_{\text{beam}}=2.807\pm0.005$ Bev/c. This was in satisfactory agreement with the results of a wire measurement to determine the beam momentum. In the event analysis P_{beam} was taken to be 2.807 ± 0.024 Bev/c for all events. The momentum spread used here was determined from the known geometrical characteristics of the beam.

The events were kinematically analyzed with the GUTS program for the following classifications:

$$\begin{aligned} p+p &\rightarrow p+p && (pp)\\ &\rightarrow p+n+\pi^+ && (pn+)\\ &\rightarrow p+p+\pi^0 && (pp0)\\ &\rightarrow d+\pi^+ \\ &\rightarrow d+\pi^++\pi^0. \end{aligned}$$

The program gave the missing mass, coplanarity, and the goodness-of-fit parameter, χ^2, for each interpretation.

To eliminate possible kinematic ambiguities, the secondary tracks were identified by ionization, either visually or by bubble counting when necessary. In this way the events were separated into the different classifications. Figures 2 and 3 show the χ^2 distributions for the pp and $pn+$ events, respectively. The $pp0$ distribution is similar to the latter. A small number of events fitted both pp and $pp0$ interpretations and were classified on the basis of coplanarity. Inelastic events with $\chi^2>5$ were remeasured. If the second measurement also gave $\chi^2>5$, the event was classified as multiple-

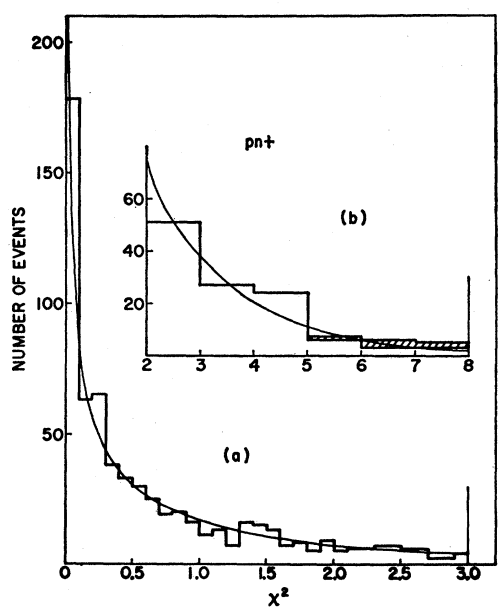

FIG. 3. χ^2 distribution for $pn+$ events. (a) Distribution for $\chi^2<3$. (b) Distribution for $2<\chi^2<8$. The shaded area shows events above the limit ($\chi^2=5$) chosen for single production. Because of kinematic considerations these events could not be accepted as double production. The curve is the theoretical distribution for one constraint.

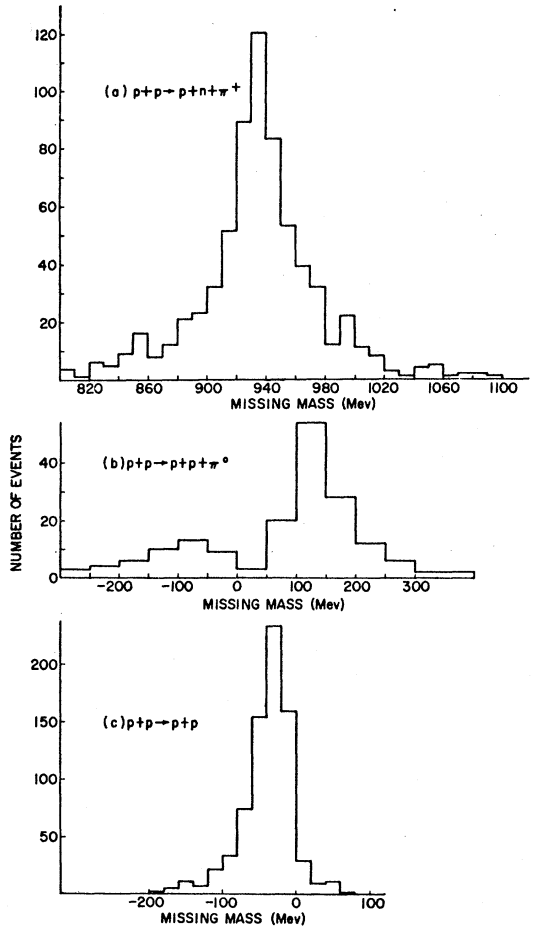

FIG. 4. Missing mass distributions for the various reactions.

pion production unless forbidden by kinematics. Figure 3(b) indicates that there is a very small overlap between the single and multiple production events with the limit $\chi^2=5$.

Figure 4 shows missing mass distributions for events identified as pp, $pn+$, and $pp0$. The widths of these

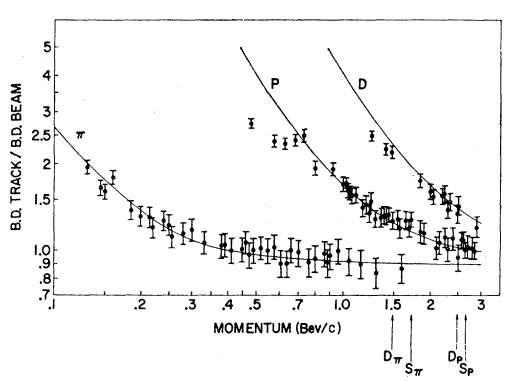

FIG. 5. Bubble density of tracks (relative to beam tracks) as a function of momentum. The curves show the expected variation of bubble density for a low $1/\beta^2$ for pions, protons, and deuterons. S_π, S_p and D_π, D_p are the upper limits of pion and proton momenta for single and double pion production, respectively.

TABLE I. Number of events and partial cross sections at 2 Bev.

Reaction	Uncorrected number of events	Cross sections σ(mb)	Errors $\Delta\sigma$(mb)
pp (elastic)	1493	19.21	0.48
$pp0$	318	3.85	0.22
$pn+$	1326	16.06	0.44
$d+$ and $d+0$	14	0.170	0.045
Λ^0Kp	11	0.018	0.005

distributions are compatible with the 35-μ measuring uncertainty.

Tracks with momenta greater than 1.2 Bev/c were identified by bubble counting. The efficacy of this technique and the possibility of distinguishing between pions and protons, up to the kinematic limits for single and double pion production, are shown in Fig. 5.

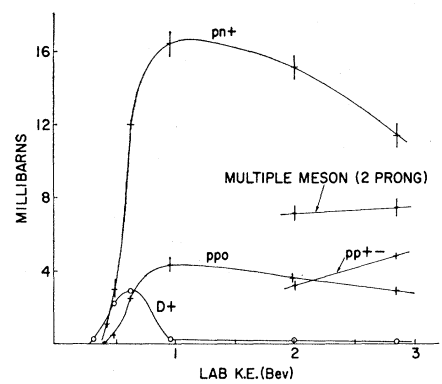

FIG. 6. Partial cross sections for inelastic processes in proton-proton collisions. The solid lines are free curves drawn through the points.

IV. CROSS SECTIONS

In the Yale portion of the scanning, the number of beam tracks passing through the fiducial volume was counted. A track length of 1628±50 m gave 2715 two-pronged events. The resulting total cross section for observed two-pronged events, based on a liquid hydrogen density of 0.0637±0.0010, was 43.8±1.6 mb. All partial cross sections will be based on this value.

Thirty-six hundred events were measured, and the number of events in each category is shown in column 2 of Table I. Column 3 gives corrected partial cross sections. The errors quoted are statistical only, and do not include the 1.5% uncertainty in hydrogen density. The elastic cross section has been corrected for small-angle scanning losses as described in Sec. V. The strange-particle cross section is based on 11 Λ^0Kp events found in the total scan of 57 300 events. This measured cross section was corrected by 40% to allow for scanning losses and escape from the chamber, and by 50% for neutral decay modes. No definite examples of Σ^+K^0p were observed.

Figure 6 shows the excitation curves for the inelastic processes in p-p collisions for various energies up to

2.85 Bev. They include results from the present work, the work of Smith *et al.*,[4] and also Batson *et al.*[9]

V. ELASTIC SCATTERING

Small-angle elastic scatters are difficult to detect in a bubble chamber, as may be seen in Fig. 7, which shows the observed small-angle differential cross section. This distribution indicates that small-angle losses are negligible beyond 4° in the laboratory ($\cos\theta_{\text{c.m.}}<0.98$).

To estimate the value of the correction for this loss, the optical model[10] was fitted to the data for $\cos\theta<0.98$. Figure 8 shows the differential cross section for all observed events, and the fitted optical curve for three values of r, where r is the radius of the absorbing disk. The best fit was obtained with $r=0.90$ f, and the resulting correction to the elastic cross section is 1.1 ± 0.3 mb.

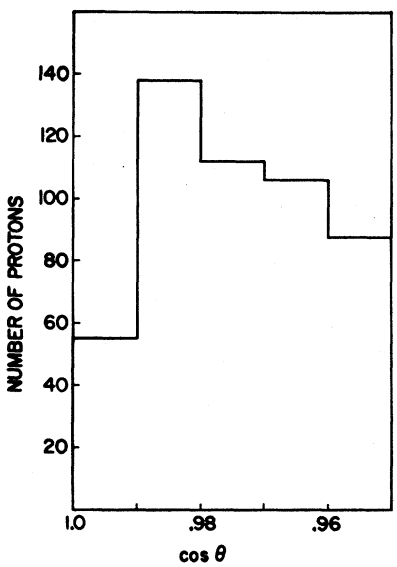

FIG. 7. Small-angle differential cross section in the center-of-mass system for elastic scattering showing scanning loss at very small angles.

This simple optical model appears to fit the data well for angles up to 50° in the c.m. system.

It was thought that the external proton beam might be partially polarized as a result of being scattered through 4° at the carbon target in the Cosmotron. In an attempt to determine this polarization, using the hydrogen as an analyzer, the number of left and right scatters was measured. The ratio $(R-L)/(R+L)$ found was 0.022 ± 0.057, which is consistent with little or no polarization of the proton beam.

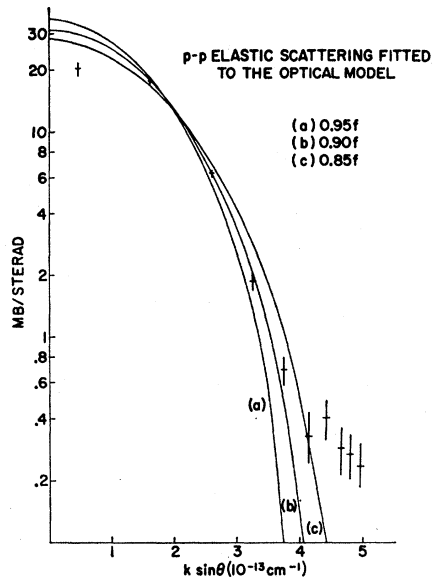

FIG. 8. p-p elastic scattering at 2 Bev fitted to the optical model. k is the wave number of the incident proton. Curves (a), (b), and (c) show the differential scattering cross sections for different values of the radius of the absorbing disk fitted to the experimental cross sections for laboratory scattering angles greater than 4°.

VI. SINGLE-PION PRODUCTION

(a) Momentum Distributions and the Isobar Model

It has become evident that the $(\frac{3}{2},\frac{3}{2})$ $p+$ resonance plays an important role in pion production in pp and

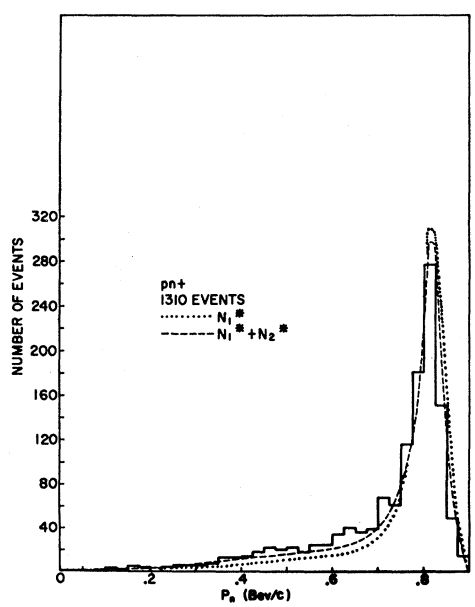

FIG. 9. Center-of-mass momentum distribution of the neutrons from $pn+$. The dotted curve is the distribution predicted by the isobar model on the assumption that isobar formation takes place through the $(\frac{3}{2},\frac{3}{2})$ resonant state alone (N_1^*); the long-dashed curve shows the distribution which also includes a contribution from the $I=\frac{1}{2}$ state (N_2^*).

[9] A. P. Batson, B. B. Culwick, J. G. Hill, and L. Riddiford, Proc. Roy. Soc. (London) **A251**, 218 (1959).

[10] S. Fernbach, R. Serber, and T. B. Taylor, Phys. Rev. **75**, 1352 (1949).

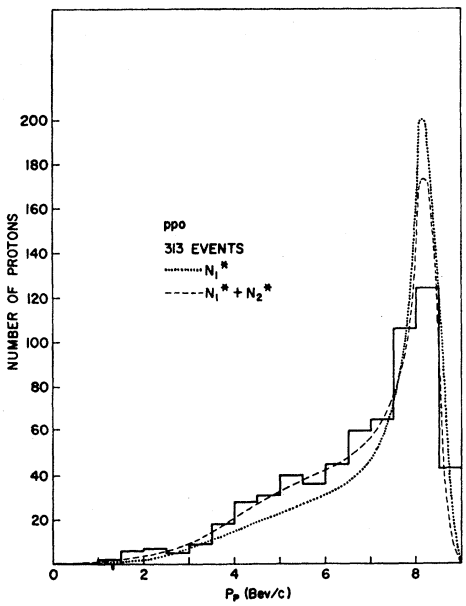

FIG. 10. Center-of-mass momentum distribution of protons from $pp0$. The curves show the predicted isobar distributions for N_1^* and an admixture of N_1^* and N_2^*.

πp collisions. Peaslee[11] has shown that if all single-pion production in p-p collisions proceeds through this state, the $pn+/pp0$ branching ratio should be 5, whereas the prediction of the statistical model is 3. The value for this ratio was determined experimentally to be 3.94 ± 0.48 at 2.85 Bev,[4] while this experiment gives 4.17 ± 0.25 at 2.02 Bev. A value less than 5 would be expected from the isobar model if there were effects

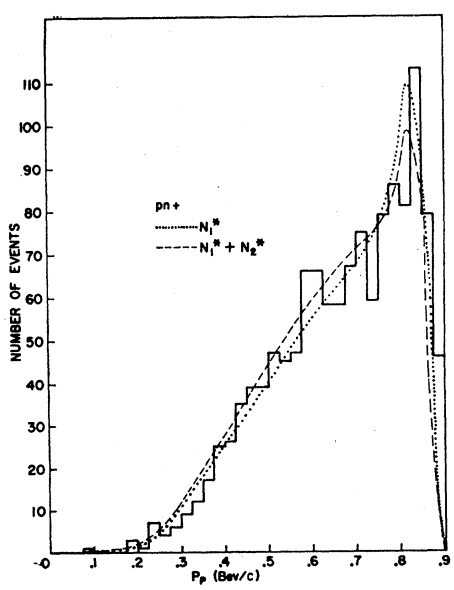

FIG. 11. Center-of-mass momentum distribution of protons from $pn+$. The curves show the predicted isobar distributions for N_1^*, and N_1^* with a contribution from N_2^*.

[11] D. C. Peaslee, Phys. Rev. 94, 1085 (1954).

from the $I=\frac{1}{2}$ resonances. The available energies in these two experiments are sufficiently high to excite these resonances. The extended isobar model proposed by Lindenbaum and Sternheimer[6] includes effects of the $I=\frac{3}{2}$ resonance at $Q_{p\pi}\simeq150$ Mev and the two $I=\frac{1}{2}$ resonances at $Q_{p\pi}\simeq430$ and 600 Mev, where Q is the kinetic energy in the pion-nucleon c.m. system. In this model the experimental branching ratio is used to determine the partial cross sections, $\sigma_{\frac{3}{2}}$ and $\sigma_{\frac{1}{2}}$, for the $I=\frac{3}{2}$ and $I=\frac{1}{2}$ isobar states (N_1^* and N_2^*). It is assumed that there is no interference between these states.

Using the experimental branching ratio, 4.17 ± 0.25, we obtain $\sigma_{\frac{3}{2}}=16.7\pm1.2$ mb and $\sigma_{\frac{1}{2}}=2.3\pm1.2$ mb, and these values are used in what follows to evaluate the experimental distributions in terms of the isobar model.

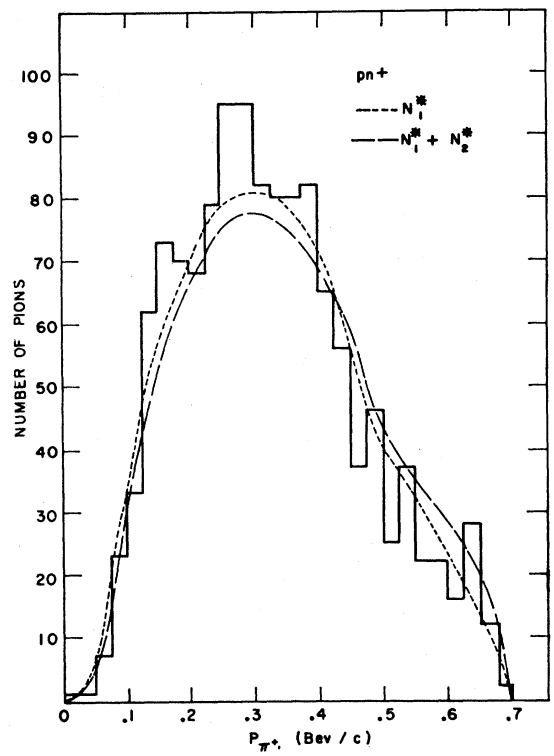

FIG. 12. Center-of-mass momentum distribution of positive pions from $pn+$. Predicted isobar curves are shown for comparison.

The isobar model for single-pion production assumes the production of a short-lived intermediate pion-nucleon state (N_1^* or N_2^*) with a recoil nucleon and the subsequent free decay of the isobar:

$$p+p\rightarrow N+N^*$$
$$\searrow N+\pi.$$

The momentum distribution of the recoil nucleon is calculated from two-body kinematics and the distributions of the decay particles are obtained under the assumption that the decay is isotropic in the isobar rest system.

The histograms in Figs. 9–13 show the experimental momentum distributions in the c.m. system for all outgoing particles from the $pn+$ and $pp0$ reactions. In these figures the momentum distributions predicted by the isobar model are shown both for pion production through N_1^* only (short dashes or dots) and for pion production with contributions from N_1^* and N_2^* (long dashes).

The neutron momentum spectrum from $pn+$ (Fig. 9) shows a sharp peak at 810 Mev/c, corresponding to the recoil from the $p+$ isobar. Similarly the proton spectrum from $pp0$ (Fig. 10) shows a peak at 810 Mev/c corresponding to recoils from the $p0$ isobar in the $I=\frac{3}{2}$ state. The N_1^* model predicts for the $pn+$ reaction that 90% of the neutrons are recoils from the $p+$ isobar, and 10% are decays from the $n+$ isobar. For the $pp0$ reaction 50% of the protons are predicted to be recoils and 50% decays from the $p0$ isobar. The decay nucleons form a low-momentum group. The

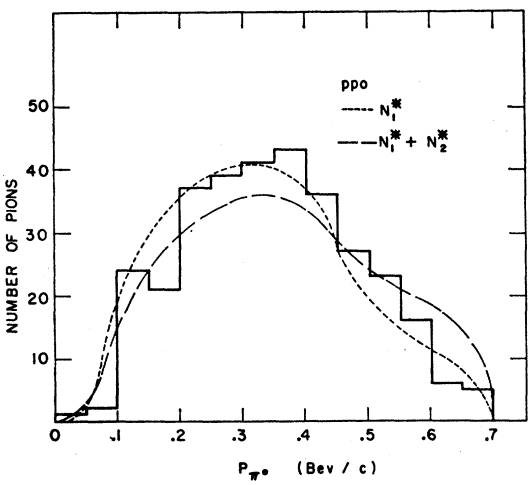

FIG. 13. Center-of-mass momentum distribution of neutral pions from $pp0$. Predicted isobar curves are shown for comparison.

effect of N_2^* is to increase the proportion of low-momentum nucleons (decays and recoils from $p0$ and $n+$ in the $I=\frac{1}{2}$ state). The histograms in Figs. 9 and 10 are in somewhat better agreement with the theoretical curves which include contributions from both isobars ($N_1^*+N_2^*$ model.)

The expected momentum distribution for protons from $pn+$ consists mainly of decays from the $p+$ isobar, and also small groups of recoils from the $n+$ isobar. Figure 11 shows that the experimental distribution is in satisfactory agreement with the prediction of the $N_1^*+N_2^*$ model.

The experimental pion momentum distributions are shown in Figs. 12 and 13, with the theoretical predictions. These distributions also appear to be in reasonable agreement with the $N_1^*+N_2^*$ curve.

Since it is clear that the $pn+$ reaction goes predominantly through excitation of the $p+$ isobar, it

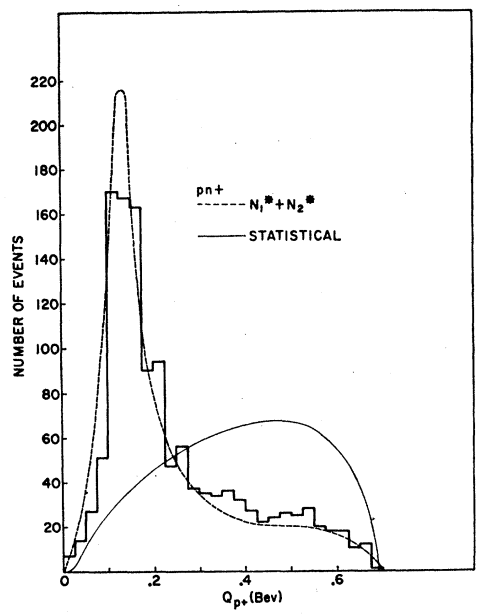

FIG. 14. Q-value distribution for $p\pi^+$ in the $pn+$ reaction. The dashed curve shows the predicted isobar distribution for pion production through both the $(\frac{3}{2},\frac{3}{2})$ and $I=\frac{1}{2}$ resonant states ($N_1^*+N_2^*$). The solid curve shows the predicted distribution for a three-body statistical model.

may be informative to study this isobar in more detail. Figure 14 shows the distribution of Q_{p+} and, for comparison, the theoretical curve for the $N_1^*+N_2^*$ model. The decay angle δ between the direction of the proton in the rest frame of the isobar and the c.m. direction of the isobar was calculated for all $pn+$ events. Figure 15 shows the decay angular distribution for all events, and for those in the Q peak (75 Mev$\leq Q<$225 Mev). The latter distribution is approximately isotropic, in confirmation of the assumption made in the theoretical

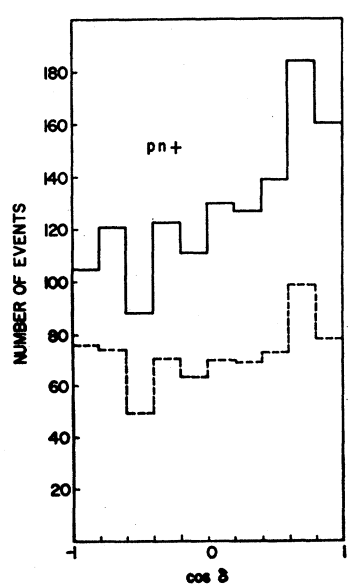

FIG. 15. Distributions of the angle δ of the pion in the rest frame of the pion and proton ($p+$) relative to the direction of $p+$ isobar in the total center-of-mass system, for the $pn+$ reaction. The solid histogram is for all events; the dashed histogram is for events in the Q_{p+} peak. ($75\leq Q_{p+}<225$ Mev.)

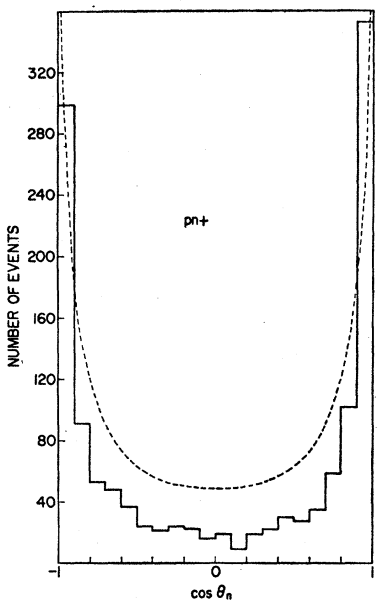

FIG. 16. Center-of-mass angular distribution of neutrons from $pn+$. The dashed curve shows the absolute differential cross sections calculated from Selleri's equations for a one-pion exchange model.

calculations of the momentum spectra of the decay particles.

(b) Angular Distributions and the One-Pion Exchange Model

Figures 16–20 show the c.m. angular distributions for the nucleons and pions from $pn+$ and $pp0$. It is seen that the nucleons are sharply peaked forward and backward, while the pions are more nearly isotropic. The nucleon distributions are strongly indicative of peripheral collisions. The predominance of such collisions is predicted by the one-pion exchange model in which it is assumed that the dominant process is the exchange of a virtual pion between nucleons, with scattering of the virtual pion by one nucleon (Fig. 21).

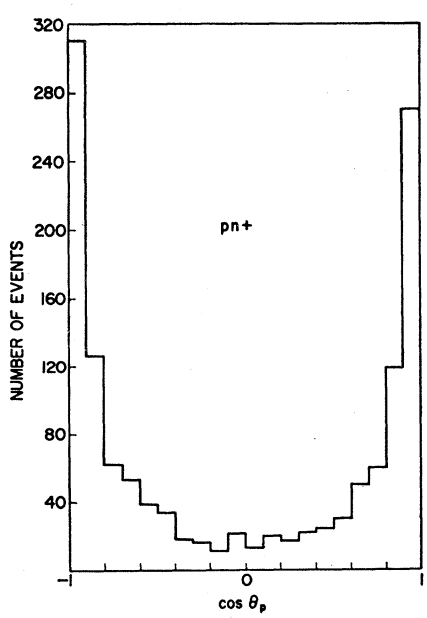

FIG. 17. Center-of-mass angular distribution of protons from $pn+$.

The theory presented by Chew and Low[12] relates the cross section for this elastic scattering to the observed pion production cross section σ. The differential cross section $\partial^2\sigma/\partial w^2\partial q^2$ for single-pion production as a function of q^2 and w^2 is measured, where q is the four-momentum transfer to the recoil nucleon and w is the total energy of the final-state pion and proton at the second vertex, in their c.m. system. The elastic scattering cross section $\sigma_{\pi-p}$ is obtained by the following procedure. The function $F(w^2,q^2)$ given by

$$F(w^2q^2)=2\pi\left(\frac{M_p}{M_n}\right)^2 \times\frac{q_{\mathrm{IL}}(q^2-q_0^2)^2}{[\frac{1}{4}w^4-\frac{1}{2}w^2(M_p^2+\mu^2)+\frac{1}{4}(M_p^2-\mu^2)^2]^{\frac{1}{2}}}\frac{\partial^2\sigma}{\partial w^2\partial q^2}$$

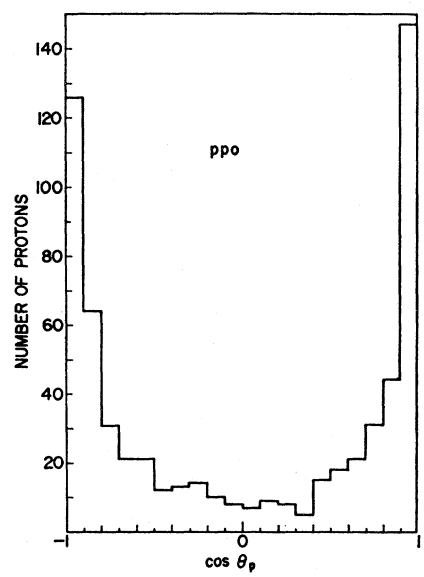

FIG. 18. Center-of-mass angular distribution of protons from $pp0$.

is calculated, where M_p is the proton mass, M_n is the mass of the recoil neutron, μ is the mass of the charged pion, q_{IL} is the momentum of the incoming proton in the laboratory system, $w=M_p+\mu+Q$, and

$$q_0^2=-(M_n/M_p)[\mu^2-(M_n-M_p)^2].$$

$F(w^2,q^2)$ is extrapolated to $q^2=q_0^2$. The scattering cross section for real pions on protons is then given by $\sigma_{\pi^+-p}=F(w^2,q_0^2)/f^2$, where f^2 is the coupling constant for charged pions to protons ($f^2=0.16$).

To test this theory, events from the $p+$ $(\frac{3}{2},\frac{3}{2})$ resonant peak (75 Mev$\leq Q<$225 Mev) were used to determine the π^+-p elastic scattering cross section, σ_{π^+-p}.

[12] G. F. Chew and F. E. Low, Phys. Rev. 113, 1640 (1959).

The extrapolation is shown in Fig. 22. The points lie approximately on a straight line, for $q^2<0.10$ (Bev/c)^2, and line (a) is a least-squares fit through these points. The value of the cross section obtained from the extrapolation is 99±62 mb. This is in reasonable agreement with the average value, 128 mb, estimated from the measured π^+-p elastic scattering cross sections in to resonant region, reported by Yuan.[13] However, it should be noted that the line (a) passes above the origin and, if constrained to pass through the origin, would give a considerably higher value for the cross section. Line (b) is a least-squares fit through the points from events not in the resonant region. A similar extrapolation, using p-p interactions at 2.85 Bev, has been made by Smith *et al.*[4]

Selleri[7] has assumed that this theory may be applied in the physical region, and has derived an expression for the absolute inelastic $pn+$ differential cross section,

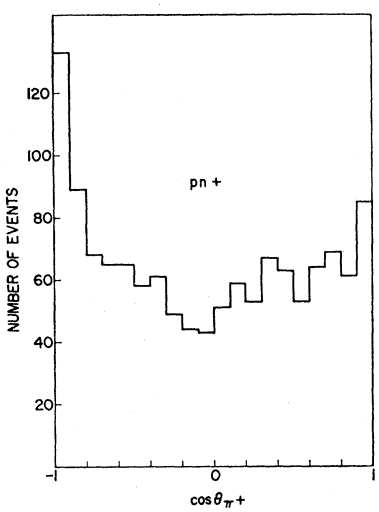

FIG. 19. Center-of-mass angular distribution of positive pions from $pn+$.

in terms of the π^+-p elastic scattering cross section. In a recent publication[14] we have compared the neutron c.m. momentum and angular distributions obtained in the present experiment with the prediction of this one-pion exchange model (absolute cross sections and angular distributions are not given by the isobar model). The shape of the theoretical neutron-momentum distribution, which is essentially determined by the shape of the π^+-p $(\frac{3}{2},\frac{3}{2})$ resonant peak, was in good agreement with experiment. The total cross section σ_{pn+}, calculated from Selleri's equation, was 23.4 mb to be compared with the experimentally determined value of 16.06±0.44 mb. The theoretical differential cross section was shown to be too high at

[13] L. C. L. Yuan, *Proceedings of the CERN Symposium on High-Energy Accelerators and Pion Physics, Geneva, 1956* (European Organization for Nuclear Research, Geneva, 1956), p. 195.

[14] W. J. Fickinger, E. Pickup, D. K. Robinson, and E. O. Salant, Phys. Rev. Letters 7, 196 (1961).

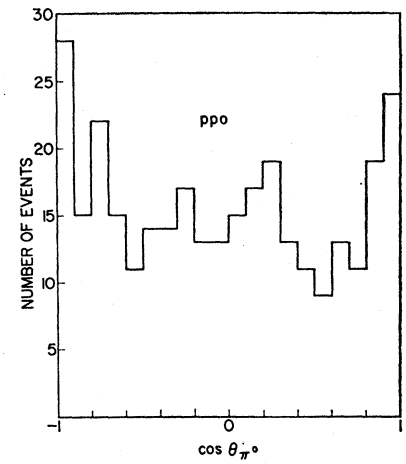

FIG. 20. Center-of-mass angular distributions of neutral pions from $pp0$.

large neutron angles. At small angles the mean differential cross section observed was in good agreement with theory, but the cross section changes more rapidly than the theory predicts. The neutron angular distribution predicted by Selleri is shown, with the experimental distribution, in Fig. 16.

In the one-pion exchange model events with $|\cos\theta_n|\sim 1$ are mainly events with small q^2. They also include a small tail of events with large q^2. q^2 is directly related to the laboratory kinetic energy, T [momentum transfer to the target nucleon is $(2MT)^{\frac{1}{2}}$]. The distribution of laboratory kinetic energies is shown in Fig. 23. Figure 23(a) shows T for the neutrons from all $pn+$ events and, for comparison, the absolute differential cross section calculated from Selleri's equation.[15] The theoretical prediction and the experimental distributions are in good agreement at the two ends of the distributions, [$q^2<0.15$ (Bev/c)^2]. At somewhat higher values of q^2 (the inner edges of the two peaks) the experimental distribution decreases more rapidly than the theoretical curve. Figures 23(b) and 23(c) show similar distributions for events in the Q_{p+} peak and events outside the Q_{p+} peak, respectively, for the BNL sample of events. The shapes of the two extreme ends of the distribution [$T<25$ Mev and $T>1.55$ Bev in Fig. 23(c)] are a consequence of phase-space limi-

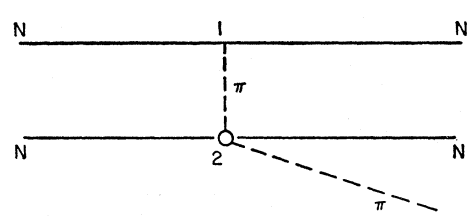

FIG. 21. Diagram showing single-pion production in $NN\pi$ through a one-pion exchange mechanism.

[15] The cross sections calculated from Selleri's equation (reference 7) have been increased by a factor of two to correct an error pointed out to us by F. Salzman (private communication).

tations. It would appear that the high-momentum transfer events (those in the valley) are primarily associated with events outside the Q peak, where a higher percentage of the neutrons are scattered particles rather than recoil particles (vertex 2 in Fig. 21). A similar effect may be observed in the kinetic energy distribution of the protons from the $pn+$ reaction, which is plotted in Fig. 23(d).

A test of the concept of scattering of the virtual pion in one-pion exchange (comparison of the angular distribution of scattered virtual pions and the known elastic π^+-p angular distribution) has been given.[14]

VII. CONCLUSIONS

The branching ratio for the $pn+$ and $pp0$ reactions, $\sigma_{pn+}/\sigma_{pp0}$ is 4.17 ± 0.25, which is somewhat lower than the value of 5 predicted for the $I=\frac{3}{2}$, N_1^* isobar mode. A small admixture of the $I=\frac{1}{2}$, N_2^* isobar is sufficient to explain this discrepancy. The theoretical curves for the c.m. momentum distributions of the nucleons given by this extended isobar model are in somewhat better agreement with the data than those given by the N_1^* model. However, the distributions are not notably sensitive to the influence of the $I=\frac{1}{2}$ resonant states.

The sharply peaked c.m. angular distributions of the nucleons in the single-pion production reactions suggest low momentum transfers characteristic of the one-pion exchange model. Comparison of the experimental angular distribution and laboratory kinetic energy distribution of the neutrons in the $pn+$ reaction with the predictions from Selleri's theory indicates reasonably good agreement for low-momentum transfers $[q^2<0.15\ (\mathrm{Bev}/c)^2]$. There is considerable disagreement for high-momentum transfers, and the predicted total cross section, σ_{pn+}, is about 50% higher than the experimental value.

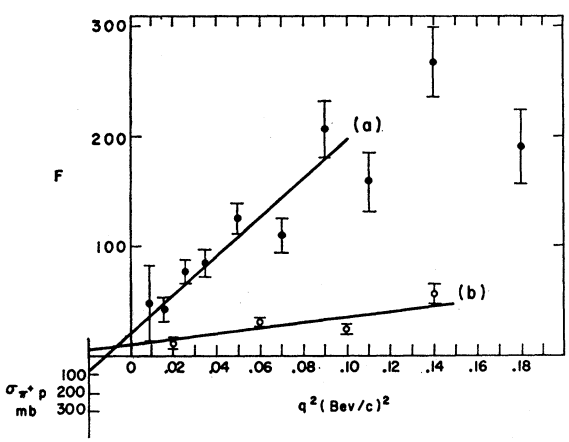

FIG. 22. Chew-Low extrapolation to obtain the π^+-p elastic scattering cross section using events from the $pn+$ reaction. Line (a) is a least-squares fit to the points ● for events from the Q_{p+} peak ($75\leqslant Q<225$ Mev) and of $q^2<0.10$ (Bev/c)^2, where q is the four-momentum transfer to the recoil neutron. Line (b) is a least-squares fit to the points ○ from events not in the Q_{p+} peak.

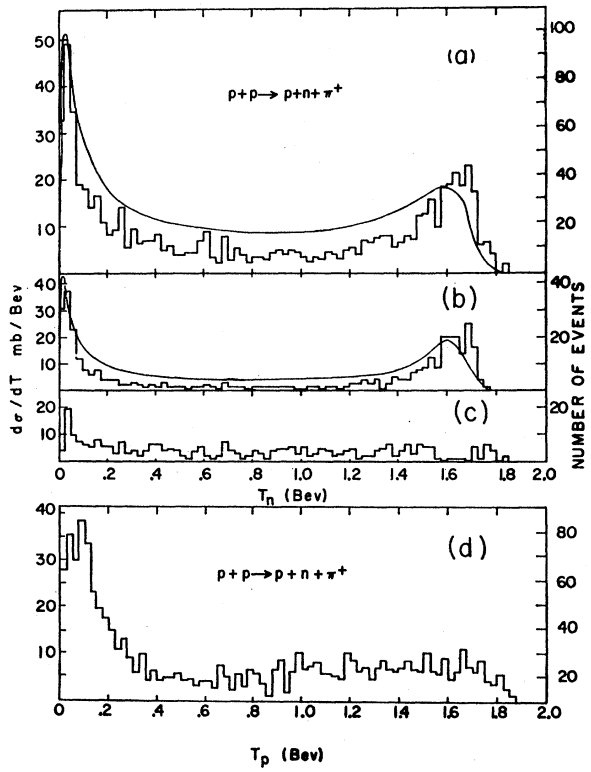

FIG. 23. Cross sections as a function of laboratory kinetic energy for the nucleons from the $pn+$ reaction. (a) shows the distribution for all neutrons; the curve gives the absolute cross sections calculated from Selleri's equation for a one-pion exchange model. (b) shows the distribution for neutrons from events in the Q_{p+} peak ($75\leqslant Q<225$ Mev). The curve shows the theoretical Selleri distribution (with integration limits corresponding to the Q selection). (c) shows the distribution for neutrons not in the Q_{p+} peak. (d) shows the distribution for all protons from $pn+$.

ACKNOWLEDGMENTS

We wish to thank the BNL Bubble Chamber group, the members of the Cosmotron staff, and also our two scanning teams for their invaluable services. We are indebted to Yam Chiu for assistance with the computations, and to J. Smith for bubble counting. W. J. Fickinger also wishes to thank his research advisor, Professor Earle C. Fowler, and Professor Horace D. Taft.